

Novel Techniques for High-Resolution Functional Imaging of Trabecular Bone

Philipp J. Thurner^{1,2,3}, Ralph Müller³, Johannes H. Kindt¹, Georg Schitter¹, Georg E. Fantner¹, Peter Wyss², Urs Sennhauser², Paul K. Hansma¹

¹ University of California Santa Barbara, Santa Barbara, USA

² Swiss Federal Laboratories for Materials Testing and Research, Dübendorf, Switzerland

³ Institute for Biomedical Engineering, ETH and University Zürich, Zürich, Switzerland

ABSTRACT

In current biological and biomedical research, quantitative endpoints have become an important factor of success. Classically, such endpoints were investigated with 2D imaging, which is usually destructive and the 3D character of tissue gets lost. 3D imaging has gained in importance as a tool for both, qualitative and quantitative assessment of biological systems. In this context synchrotron radiation based tomography has become a very effective tool for opaque 3D tissue systems. Results from a new device are presented enabling the 3D investigation of trabecular bone under mechanical load in a time-lapsed fashion. Using the highly brilliant X-rays from a synchrotron radiation source, bone microcracks and an indication for un-cracked ligament bridging are uncovered. 3D microcrack analysis proves that the classification of microcracks from 2D images is ambiguous. Fatigued bone was found to fail in burst-like fashion, whereas non-fatigued bone exhibited a distinct failure band. Additionally, a higher increase in microcrack volume was detected in fatigued in comparison to non-fatigued bone. Below the spatial resolution accessible with synchrotron radiation tomography we investigated native and fractured bone surfaces on the molecular scale with atomic force microscopy. The mineralized fibrils detected on fracture surfaces give rise to the assumption that the mineral-mineral interface is the weakest link in bone. The presented results show the power of functional micro-imaging, as well the possibilities for AFM imaging (functional nano-imaging) in this context.

Keywords: Imaging, Image Processing, Micro-Computed Tomography, Synchrotron Radiation, Bone, Nano Composite, Image Guided Failure Assessment, Microdamage, Atomic Force Microscopy,

1. INTRODUCTION

Bone belongs to the best investigated biological materials due to its primary function of providing skeletal stability and load carrying capacity. Bone is susceptible to different local stimuli including mechanical forces and has great capabilities in adapting its mechanical properties to the changes in its environment. Nevertheless, aging or hormonal changes make the bone weak, and it is losing its ability to appropriate remodeling. Therefore, bone research is primarily motivated by the social impact and the immense costs in health care associated with osteoporosis (1, 2). Osteoporosis results in bone loss and deterioration in trabecular architecture causing the decrease of bone strength, and the concomitant increase in fracture risk. Due to the emergence of accurate and precise bone densitometry over the last two decades, bone density has been a primary endpoint in osteoporosis diagnosis and monitoring. Where strong correlations between bone density and mechanical properties of trabecular bone have been demonstrated for large populations using power-law regressions (3-9). Changes in density can explain the variation of trabecular bone strength on an individual basis only on a limited basis, leaving sometimes up to 90% of the strength variation unexplained (10). Thus, accurate diagnosis in a clinical environment based solely on bone densitometry proves to be difficult. The relative contribution of bone density, microarchitecture and local tissue properties, a complex referred to as bone “quality”, to the mechanical stability of bone is poorly understood. Bone quality typically entails the following constituents; bone mineral density (BMD), bone microarchitecture, bone cell distribution (i.e. osteocytes, osteoblasts and osteoclasts), the distribution of microcracks or microdamage and the quality of the underlying organic bone matrix.

Bone tissue is extensively studied with micro-computed tomography (μ CT) and synchrotron radiation based μ CT (SR μ CT). Tomography using X-rays is a well established technique that is also applied to extended systems like body parts or whole organs of human beings (11) and to systems below micrometer scale such as individual biological cells (12) using the same principles at different levels of spatial resolution. Consequently, SR μ CT allows investigations of

tissues and organs in a hierarchical fashion – from human, to organ, to tissue and down to the individual cell over more than 6 orders of magnitude. Moreover, SR μ CT is non-destructive allowing multiple time-lapsed imaging of samples. This is especially important for functional imaging of tissue related to biomechanics and functional adaptation of cells to mechanical loading and displacement, referred to as mechanobiology. Currently the spatial resolution limit for hard X-ray tomography is around 0.1 μ m. For higher resolution other techniques have to be utilized, one of the most prospective ones being atomic force microscopy (AFM), offering resolutions even on the nanometer scale. Similarly as Tomography AFM is a technique that can be potentially combined with in situ experiments, i.e. allowing for functional imaging on the nanometer scale.

Using both SR μ CT and μ CT, bone density and microarchitecture are readily accessible; whereas, other parameters of bone quality have not been investigated to the same extent. However, they play an important role for bone stability and remodeling and have to be included into bone failure analyses. Microcracks caused by daily exercise are present even in healthy bone (13). As long as the density and magnitude of such cracks stays under a certain threshold, there is no significant change in bone strength; however, if the microcrack density and magnitude reach a certain threshold, there is a high probability for global failure (14). Thus, it is clearly beneficial to assess further bone quality parameters by μ CT. Due to their size, microcrack and cell density are parameters only detectable by SR μ CT. Even the spatial resolution of the current SR μ CT-systems does not seem to cover the numerous aspects of bone quality. Therefore AFM can be used to perform complementary studies on the resolutions not accessible by SR μ CT, uncovering collagen fibrils and even mineral particles on native and fractured bone surfaces.

Different studies have shown that including micro- and ultrastructural bone properties in the analysis of bone strength fracture risk on the statistical basis is beneficial. However, mechanistic or constitutive modeling so far has not been fully successful, as the observation of actual bone failure modes was limited and also the individual molecular constituents of bone are not fully known. Consequently, image guided failure assessment (IGFA) combining mechanical testing and micro-computed tomography was developed (15-17). With this method it is possible to investigate bone failure in a time-resolved fashion where the actual “3D movie” of the failure process can be retrieved, step by step. IGFA has been only used in combination with μ CT so far. SR μ CT is believed to enhance insight into the failure process at the micro and ultrastructural level. The extraction of bone quality parameters (microcrack and cell density) allows investigating microcrack initiation and evolution in 3D. The possibility to measure the cell activity in bone allows gaining insights into remodeling of healthy and diseased bone; however, no stains have been adapted or developed for cell imaging using SR μ CT. AFM imaging on the other hand can help to identify and probe the different molecular building blocks of bone.

The work presented in this communication is based on the general idea to provide tools for qualitative and quantitative characterization of bone tissue using synchrotron light AFM. These tools include the visualization and quantification of microcracks in bone to study bone failure, the presentation of a device for IGFA at the synchrotron radiation source, and visualization of native and fractured bone surfaces with nanometer spatial resolution. The device for IGFA is validated, comparing the results to conventional mechanical testing. The uncovered features, microcracks and microfractures, are discussed in the context with the 2D tools conventionally used for the classification and quantification of microdamage. A preliminary algorithm for microcrack quantification is introduced. AFM images show the topography of bare and mineralized collagen fibrils on native and fracture bone surfaces respectively. Finally, the comparison between the failure of fatigued and non-fatigued trabecular bovine bone shows a higher increase in the accumulated microcrack and microfracture volume in fatigued bone.

2. MATERIALS AND METHODS

Bone Sample Preparation for IGFA

Slabs were cut from a distal bovine femur using a band saw (FK23, Bizerba GmbH & Co. KG, Balingen, Germany), the slab surface was perpendicular to the principal loading axis. Using a diamond trephine (MedArtis AG, Munich, Germany) and a drill press (Promac 212, Tooltek Co. LTD., Taichung Hsien, R.O.C.), cylindrical bone specimens of 3.7 mm diameter were cored from the slabs. The cores were cut to 4 mm long samples with a precision blade saw (Isomet 5000, Bühler LTD., Lake Bluff, Michigan, USA). Throughout the preparation procedure, the bone samples were constantly irrigated with phosphate buffered saline (PBS) (pH 7.4) to cool them and preserve the bone properties during the production process. Bone marrow was extracted from the cylinders using a 0.2% handsoap (Johnson Diversey, Sturtevant, USA) in purified water and an ultrasonic bath. The samples immersed in the handsoap solution were placed in ultrasonic bath for a period of 90 min, keeping the water temperature constantly below 40 °C. The solution was exchanged and the samples were rinsed with ultra-pure water. This process was repeated typically 5 times

until no more bone marrow was visible under a light microscope. After marrow extraction, the samples were kept in PBS at 4 °C. For mechanical testing and IGFA, the samples were glued onto 1 mm thick brass plates, 4 mm in diameter using cyano-acrylate super-glue (Loctite 431, Henkel KgaA, Düsseldorf, Germany). The samples were exposed to air until the glue was dry and placed into PBS for re-hydration. Bone samples were subjected to mechanical testing within the next 6 h. For IGFA in combination with SR μ CT imaging, two similar samples were selected by scanning them with a desktop tomography system (μ CT 40, Scanco Medical AG, Bassersdorf, Switzerland). The selection was based on similar sample morphology, i.e. the values for relative bone volume (BV/TV), bone surface (BS) and structure model index (SMI) were used.

Table 1: Morphological parameters used to select two similar samples used for IGFA.

Sample / Description	BV/TV [%]	BS [mm ²]	SMI
Sample A (not fatigued)	23.45	140.30	0.77
Sample B (fatigued)	22.99	141.29	0.68

BV/TV indicates the total amount of bone within the cylinder, the BS is a measure for the total surface of the specimens and the SMI gives their mean shape, it is a parameter indicating whether the observed trabeculae are rather rod or plate-like (18). The values for the selected samples are given in Table 1. The SMI of 0.7-0.8 indicates that both samples are a hybrid case between plates and rods, being closer to the plate-like shape. The two selected samples were stored in PBS soaked gauze at -20 °C until the IGFA experiment was performed. Then the samples were thawed immersing them in PBS kept at room temperature.

Bone Sample Preparation for IGFA

Trabecular parts of bovine vertebrae were diced into blocks of 4x4x5 mm³ under constant irrigation using a bone bandsaw (Marmed Inc., Cleveland, OH, USA), and the marrow was removed with pressurized water (Waterpik Technologies, Fort Collins, CO, USA). For native bone surface investigations a bone cube with an accessible native surface was selected and glued to an AFM sample disk using epoxy resin (2-Ton Clear Epoxy, Devcon, Danvers, MA, USA). For fracture surface investigations the outside surface of a bone cube was stained with Coomassie Blue R (Sigma-Aldrich, 0.2g/ml) in Na-buffer (150mM NaCl, 10mM Hepes, pH 7.0) for 5 minutes, and the samples were rinsed in Ca-buffer (110mM NaCl, 40mM CaCl₂, 10mM Hepes, pH 7.0) to remove excess stain. Subsequently, a stained bone cube was soaked in Ca buffer for 5 minutes, then clamped in a vice, with the bone load axis parallel with the vice grip edge, and half of the block extending from the vice was clamped into a second vice. The block was then pulled apart, i.e. the bone block was fractured in tension. The two pieces were immediately rinsed off briefly in HPLC grade H₂O (EMD Chemicals Inc., Gibbstown, NJ), blotted dry on a Kimwipe from the side not exposed by fracture, and separately placed in centrifuge tubes with a small wad of Kimwipe at the bottom. The blocks were centrifuged for 5 minutes to remove any residual buffer and avoid artifacts from salt residues, and desiccated in vacuum for at least 30 minutes. All these steps are designed to prevent modifications of the fracture surface after the fracture event, in particular the formation of salt crystals from the buffer. To find an area suitable for AFM imaging, the dried cube was placed under a dissection microscope. The Coomassie stain let us clearly distinguish between stained external surfaces (blue) and un-stained fracture surfaces (white). For AFM, it is important to choose a sample surface that is reasonably smooth. Areas, which appeared translucent and smooth, turned out to be the most suitable for AFM investigation. Once identified, a trabecula with a promising fracture surface was removed with a scalpel, and embedded in epoxy resin (2-Ton Clear Epoxy) in a custom-made AFM sample disk with a well in the center, with the surface to be investigated facing upward and exposed roughly parallel to the disk.

SR μ CT

Tomography experiments were performed at the MS beamline (19) at the SLS of the Paul Scherrer Institute (PSI). For the IGFA experiments a photon energy of 20 keV was used. The pixel size in each of the recorded projections was 3.5 μ m. These data were subsequently binned by a factor of two prior to the reconstruction in order to increase the signal to noise ratio (20). Each sample had to be scanned 3 times at different heights at every compression step recorded during IGFA, since the used X-ray beam was less than 2 mm in height. The used tomography setup had a field of view (FOV) of 7 mm by 7 mm. Thus, the tube made of Torlon 4203 (Solvay S.A., Brussels, Belgium), a poly-amid-imide, around the sample with an outer diameter of 10 mm was not entirely in the FOV of the detector, i.e. local tomography was performed. This resulted in an offset of reconstructed absorption values and in a typical bright ring shaped artifact or two half ring shaped artifacts within reconstructed slices (21).

Image Guided Failure Assessment

For IGFA experiments samples were inserted into the sample chamber of the newly developed in situ mechanical loading and staining device (IMCSD) (22). After insertion into the IMCSD sample chamber, where the specimens were kept immersed in PBS, a preload of 5 N was applied, and the samples were preconditioned by compressing them seven times to 0.3% strain. For sample B (Table 1) the preload was considerably higher, namely 10 N. Prior to any mechanical testing the radiographic images were used to measure the exact sample height, resulting in 4071.5 μm for sample A and 4175.4 μm for sample B. After the preconditioning, the elastic modulus was determined by compressing the specimen up to 0.3%. Sample B was additionally fatigued applying 3500 displacement cycles between 0% and 0.5% strain. After each 500th cycle the dynamic compression was stopped and a hysteresis curve was recorded compressing the sample to 0.5% strain. Fatigue was defined as a 10% reduction in modulus. For IGFA both samples were tomographically scanned at 0%, 1% and 2% strain. The fatigued sample without strain was scanned twice, before and after the application of the dynamic displacement cycles. During all IGFA experiments the applied displacements were crosschecked with values derived from radiographic projections.

Data Processing of SR μ CT Data

The datasets retrieved from the bone samples at the different heights were joined to a single dataset at each compression step. Then a cylindrical ROI was chosen in order to exclude the artifacts arising from the local tomography performed. Subsequently the dataset was smoothed applying a 3D Gaussian filter (sigma 1.2 voxels on a 3x3x3 voxel base) and thresholded using an automated adaptive thresholding algorithm. For visualization the binarized data were segmented in endplates and bone in a semi-automatic manner, and the binarized datasets were all subjected to a component-labeling algorithm in order to remove all but the largest component. Subsequently the datasets were aligned at the lower, not-moving endplate using a cross-correlation routine.

Atomic Force Microscopy

Samples were set up in an AFM (Multimode, Veeco Inc., Santa Barbara, CA, USA) equipped with a video microscope (OMV, Veeco). For imaging of fractured surfaces a silicon, tapping in air (RTESPW) cantilever was mounted in a multimode glass liquid cell (23, 24) fitted with an S-shaped silicone O-ring (Veeco). A dry Nitrogen source was furnished from a Dewar filled with liquid nitrogen, a 20 Ohm, 25W power resistor, and a Variac variable transformer (Staco Energy Products Co., Dayton, OH, USA). The Dewar was connected to the liquid cell via several meters of tubing to allow the gas to equilibrate to room temperature before entering the fluid cell. The voltage was set to 7V AC during imaging. The use of dry gas during AFM imaging removes the hydration layer on the sample surface, which can affect the sample tip interaction and degrade spatial resolution. The fractured surface was imaged in tapping mode and dry N₂ gas at a scan rate 1 Hz. The whole bone cube used for imaging of native bone surface was in air using a coated microlever (Model # MLCT-AUHW, Veeco) at a scan rate of 2 Hz. The AFM images of height and deflection of each sample shown were combined to a 3D surface representation using commercial software (Nanoscope Software, Veeco).

3. RESULTS AND DISCUSSION

The IMCSD was developed to perform in-situ loading experiments of trabecular bone specimens at the Materials Science (MS) beamline of the Swiss Light source (SLS) (25), including cyclic loading of biological systems in a well-defined hydrated environment. The constraints for the realization of such an instrument include limitations on the weight of the device since it must be carried by the high-precision sample manipulator stage. Similarly the outer geometry is constrained since the device must fit onto the stage bringing the sample into the beam and rotating it during a tomography scan. In order to have displacement control with the possibility to apply dynamic loads a piezoelectric actuator with large displacement has been chosen for the displacement exerting part. 3D design drawings, as well as a photograph of the device in operation of the IMCSD are shown in Figure 1. As can be seen it consists of three major parts: the sample chamber, the actuator housing, and the mechanical guides. The sample chamber consisting of brass and a radiolucent plastic tube, made of Torlon is in the lower part. It is directly screwed onto the tomography sample handler. The actuator housing and mechanical guides are in the upper part and connected via a bearing. Once the sample chamber is screwed to the actuator housing they can both rotate as a unit about the fixed guides, driven by the rotation axis of the sample handler. The valves attached to the sample chamber are used for applying physiologic fluid to sample. The whole device was previously validated for mechanical testing (22).

Figure 2 shows 3D visualizations of the whole as well as a detail of the bone sample subjected to IGFA that was not fatigued. This sample exhibits a fracture band at 2% strain ranging through the whole sample from the top left to the bottom right, as indicated by the black lines in Figure 2. Especially the detail in the same figure shows the power of IGFA in combination with SR μ CT: microscopic cracks, i.e. microfractures and microcracks are uncovered in a 3D manner.

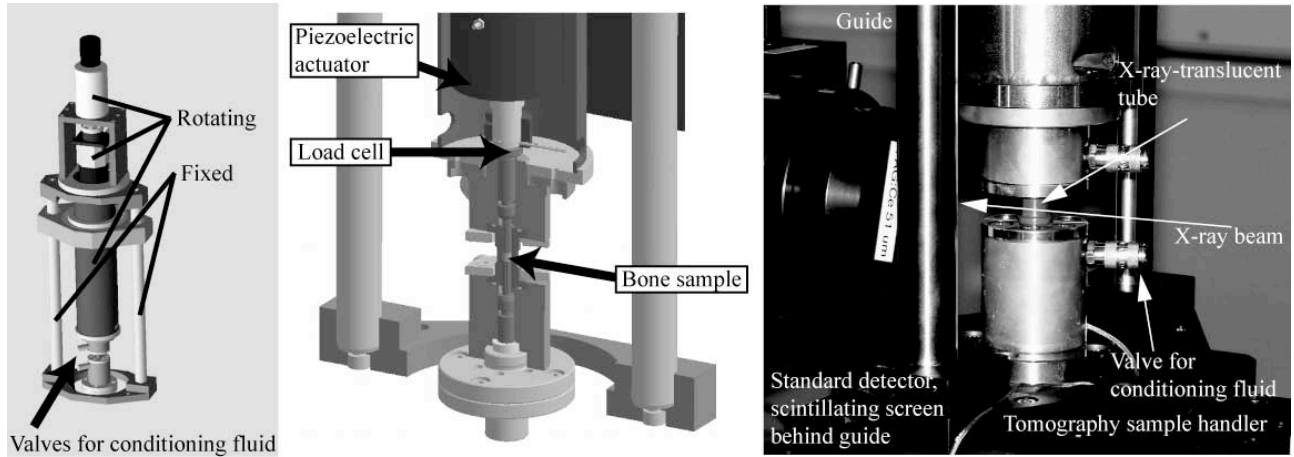


Figure 1: 3D design drawings of the whole IMCSD device (left), and the sample chamber (middle), which is screwed to the actuator housing and the tomography rotation stage. A photograph of the device in operation is given (right).

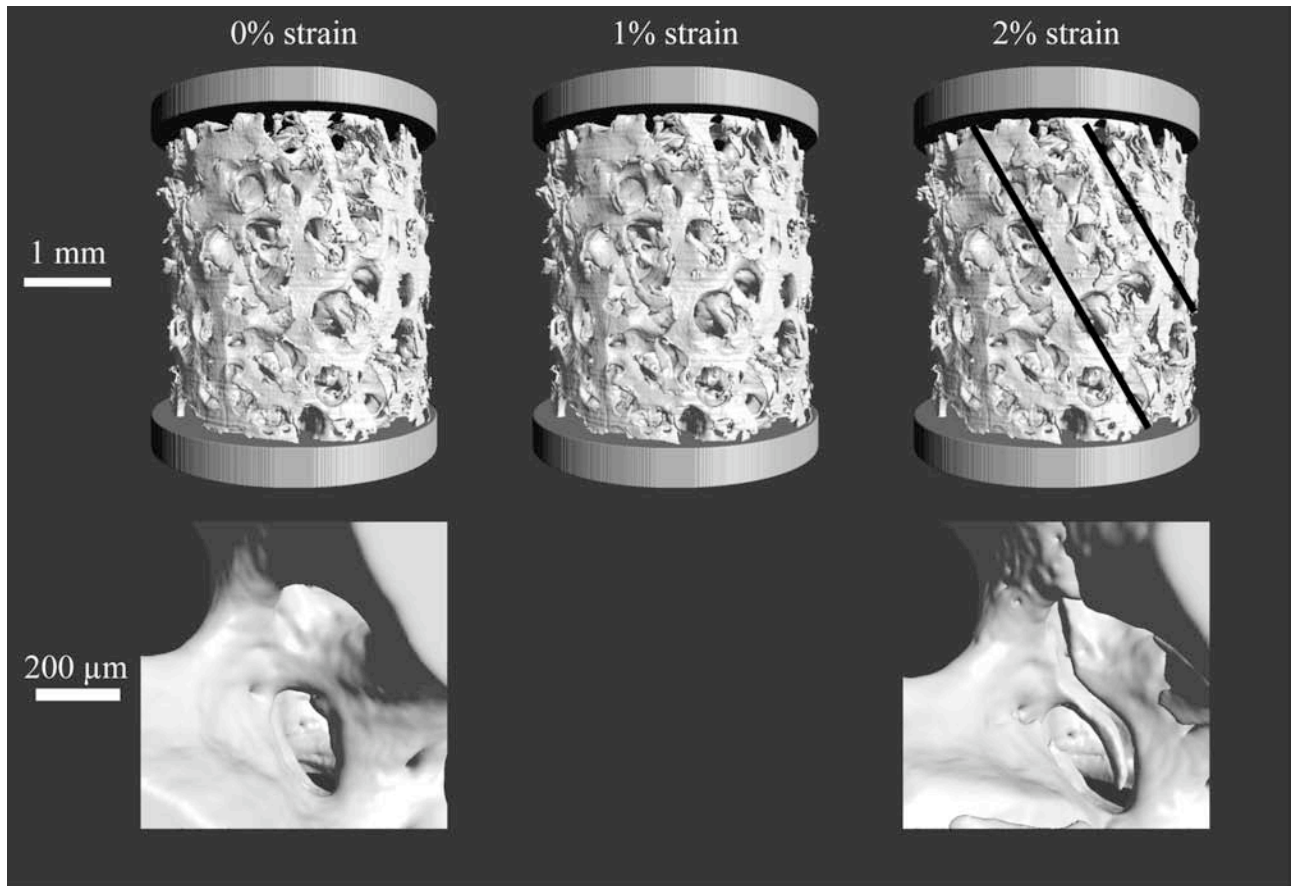


Figure 2: 3D visualization of a detail and the whole non-fatigued bone sample (sample A, Table 1) subjected to IGFA at different compression steps. The sample shows a fracture band going diagonally from the upper left to the lower right through the sample (indicated with the black lines, the failure band is situated in between them). The detail shows the microcrack formation. Data acquired at the MS beamline (SLS) at the photon energy of 20 keV.

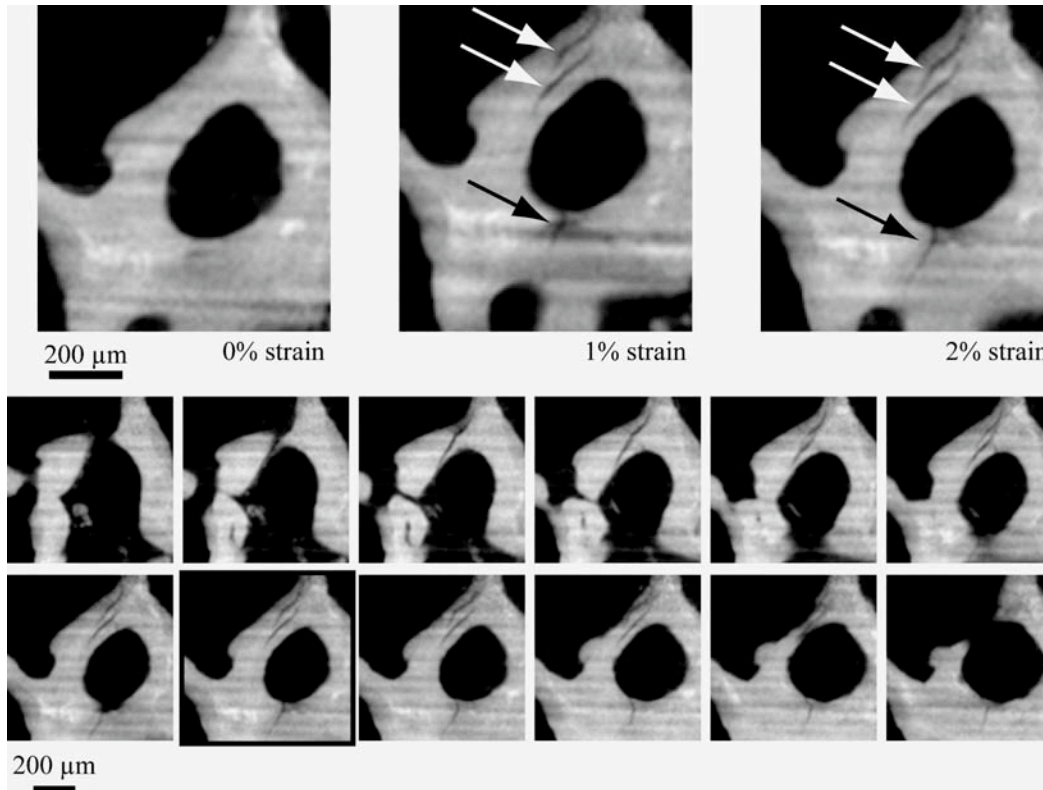


Figure 3: Detail of virtual, 7.5 μm thick sections through sample A at the different compression steps (top). In the images two internal (white arrows) and one surface connected (black arrow) microcrack can be distinguished. The classification internal is actually misleading as shown in the image series presented at the bottom (corresponding slice to the one at top has a black frame). In fact the two internal cracks are one crack extending over a whole trabecula being connected to the bone surface, i.e. a microfracture. The horizontal streaks seen in the slices are due to features present in the incoming X-ray beam. Data were acquired at the MS beamline (SLS), photon energy 20 keV.

In order to quantify the observed microcracks and microfractures in bone an algorithm for their detection was developed based on the morphological dilation and erosion procedure. The algorithm was performed on the binarized bone structure. First the morphological dilation was performed a few times. The exact number of repetitions is dependent on the maximum crack thickness, which shall be detected. This crack thickness can be estimated as follows: each dilation step closes a crack up from two sides, i.e. it detects cracks with a thickness of two voxel edge lengths. Subsequent to the dilation operations the morphological erosions were performed. The number of erosion steps is the same number as dilation steps plus one, in the case presented here 7 dilation and 8 erosion steps. Finally the retrieved volume is used as a mask on the inverted bone volume data. Left after the masking procedure are the cracks, but also internal voids, and depending on the number of dilations performed also a considerable volume on the bone surface. The latter is selected due to the trabecular morphology. This means that the quantitatively detected crack volume is always higher than the actual crack volume. It is, however, still possible to compare the development of crack volume in a specimen subjected to a series of compression steps as done during IGFA using the retrieved crack volume at zero strain as the baseline. Besides the crack detection another important parameter of interest is, whether the microcracks are in connection with the bone surface or if they are purely internal. The reason for this is due to the classical 2D methods used to study microcracks, i.e. histology and microscopy. In such investigations microcracks are usually classified for quantitative analysis as either internal or surface connected cracks (26-28). In compact bone the number of surface connected cracks is small (29). Thus an algorithm was developed dividing the cracks into internal and surface-connected ones and computing their respective volumes. Cracks that range through a whole trabecula are usually not considered as microcracks but are referred to as microfractures (30). The fact that the conventional classification of microcracks and microfractures from 2D images is ambiguous is proven in Figure 3.

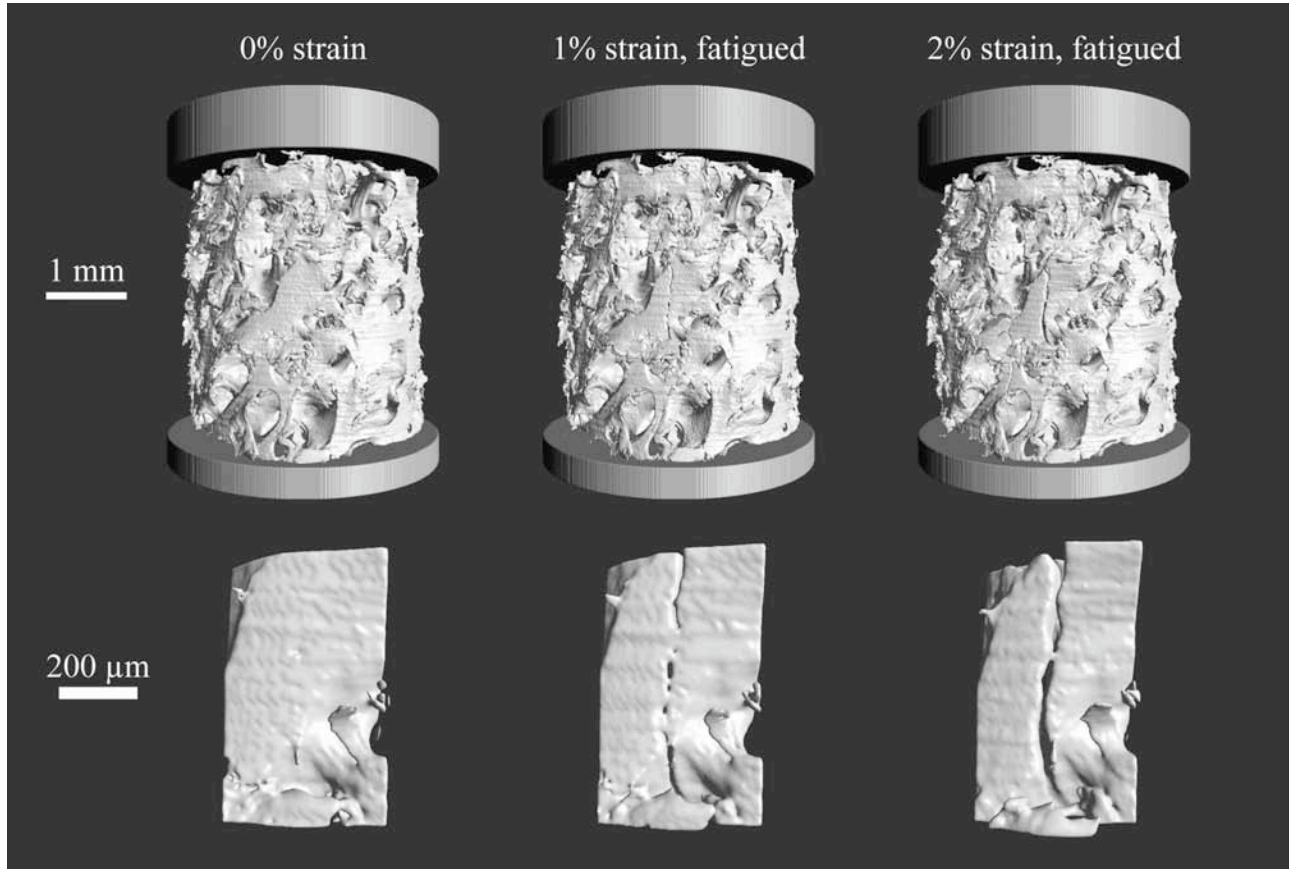


Figure 4: 3D visualization of a detail and the whole fatigued bone sample (sample B) before and after fatigue at different strains. The sample shows a burst-like fracture behavior. The detail shows the microcrack located in the middle of the 3D visualization of the whole sample. Even at 2% strain the two crack surfaces are not completely disrupted but are still connected, presumably by bone ligaments (un-cracked ligament bridging). Data acquired at the MS beamline (SLS) at the photon energy of 20 keV.

Here virtual 2D cuts through the sample are displayed: at the top a virtual cut through similar regions of the sample at zero, 1% and 2% strain is shown. Cracks indicated by the arrows are forming at 1% strain and are propagating increasing the strain to 2%. The three cracks that can be distinguished from the virtual cut would be classified as two internal microcracks (white arrows) and one microcrack connected to a bone surface (black arrow). Figure 4 shows 3D visualizations of a detail as well as the whole bone sample subjected to IGFA that was fatigued prior to compressing to 1% and 2% strain. Interestingly, no crack formation could be observed directly after subjecting the sample to the dynamic displacement cycles. The structure of the bone has changed since the elastic modulus of the sample decreased by about 10%.

Table 2: Quantified crack volume in mm³ applying the crack detection algorithm with 7 dilation and 8 erosion steps, resulting in a maximum detectable crack thickness of about 100 μm.

Sample / Description	Sample A (not fatigued)	Sample B (fatigued)
Internal cracks at 0% strain	0.007	0.002
Internal cracks at 1% strain	0.002	0.003
Internal cracks at 2% strain	0.002	0.005
Surface connected cracks at 0% strain	1.280	0.976
Surface connected cracks at 1% strain	1.196	1.010
Surface connected cracks at 2% strain	1.539	1.490

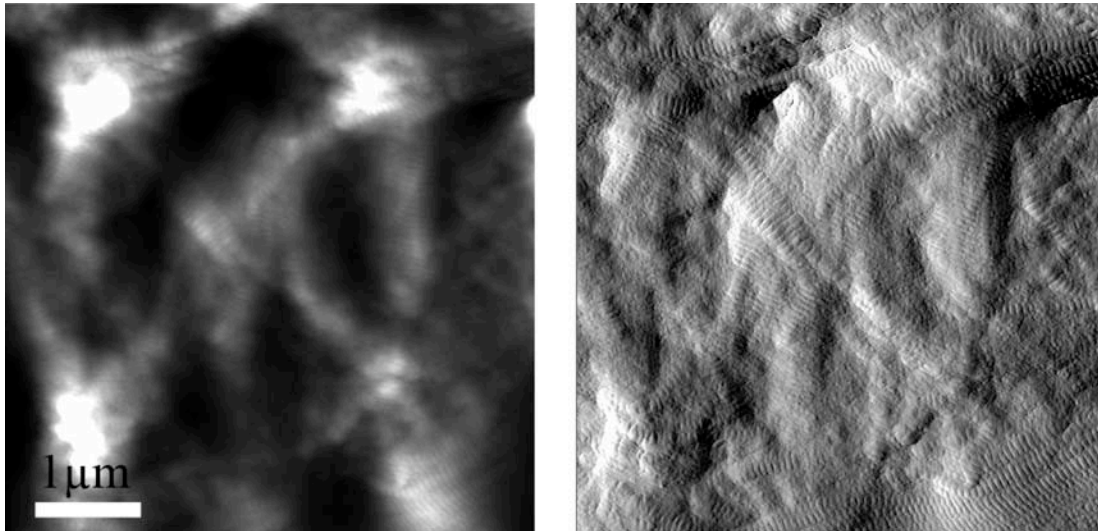


Figure 5: AFM height (left) and deflection (right) images of a native bovine trabecular bone surface. Bare collagen fibrils with the typical corrugation of 67 nm are clearly visible.

It might be that most of the cracks seen upon compressing the sample up to 2% strain were already there or at least initiated but were beyond the spatial resolution of the acquired tomogram. The sample visualized in Figure 4 fails in a burst-like fashion, in contrast to the band-like failure of the sample that was not fatigued. It can be seen that the two pieces, that seem to shear off from each other are not fully separated even at 2% global strain. Filamentous features can be seen to span the crack. This finding is an indication for un-cracked ligament bridging, which was so far only observed in SEM images of bone (31). In terms of the detected crack volume the majority of the crack volume (99.99%) is actually connected to the bone surface. Both samples display an increase in crack volume with increasing strain. The increase in crack volume is almost twice as high in the fatigued sample compared to the non-fatigued sample. The result of the crack detection algorithm is summarized in Table 2 for both samples. The fact that the values for internal crack and surface connected crack volumes are higher at zero strain than at 1% strain for the non-fatigued sample can be explained by a worse SNR in the data acquired at zero strain, which results in a more rippled surface and thus also a higher number for the detected crack volume. It should be noted that the crack surface would be a more useful parameter since it directly relates to the energy dissipation.

Overall the 3D visualization of the cracks, i.e. microcracks and microfractures, without staining is a breakthrough. For the first time these features can be non-destructively detected in a 3D manner (cp. Figures 2-4). The result shows that the majority of the detected cracks are connected to the bone surface, suggesting that “internal” cracks frequently reported in histological post-hoc analyses of microdamage are rather an artifact emerging from the technique used, rather than a true finding. Interestingly, a considerable number of cracks are per definition microfractures, since they extend through an entire trabecula. Looking at the virtual sections of such microfractures, these were classified as microcracks (cp. Figure 7). Thus the classification of a microfracture and a microcrack from the 2D image is ambiguous, depending on the location and the direction of a given section, a microfracture might be classified correctly or not. Moreover, the diffuse, crosshatched, and confined cracks found in the 2D analyses can also be explained by the limited assessment of the cracks using the conventional techniques. Despite the fact that the used detection algorithm for crack detection is not devoid of errors so far the surface-connected crack volume does also increase much more than the internal cracks. Since the baseline of cracks, due to detected artifacts, can be assumed to stay more or less constant this is an indication that the amount of surface-connected cracks is much higher than the number of internal cracks. The crack detection algorithm must be further developed in order to exclude artifacts to give a clear picture of the evolution of microcracks and microfractures. Then also the crack surface can be quantified in a 3D manner. The fact that an indication of un-cracked ligament bridging can be seen is surprising and has to be validated. This makes the technique as a whole even more promising. Since the effect is known to increase the fracture toughness IGFA using SR μ CT might be a way to study the effect in 3D, relating it to healthy or diseased bone status. Besides being a toughening mechanism the un-cracked ligament bridging could be an effect needed for bone repair by osteoblasts and -osteoclasts as it provides information of broken bone pieces that need to be mended together. It might be that the absence of such ligaments prevents the correct repair of bone and thus trabeculae are irrecoverably lost.

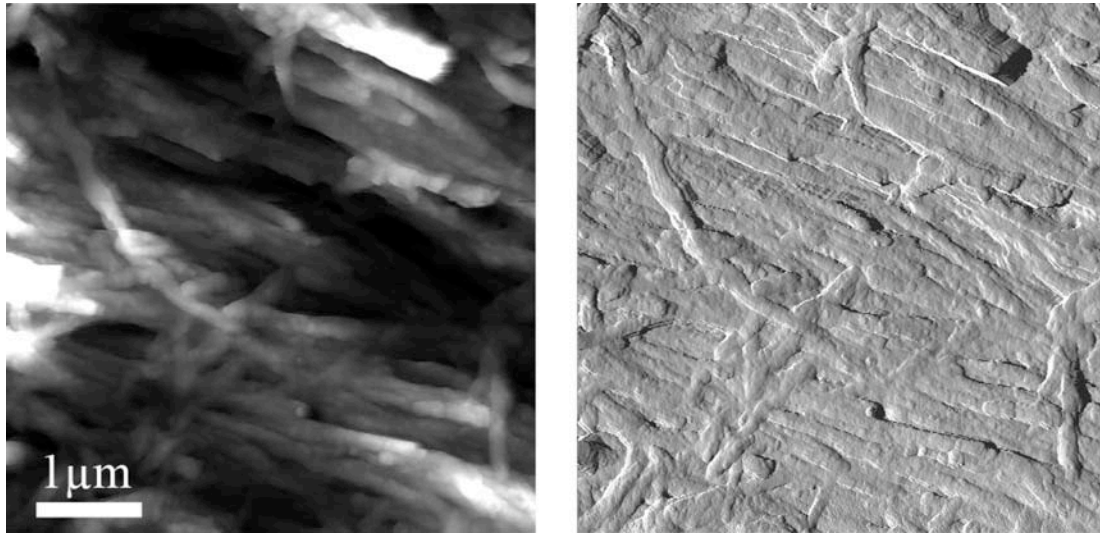


Figure 6: AFM height (left) and deflection (right) images of a fractured bovine trabecular bone surface. Collagen fibrils are coated with knobby features, presumably mineral crystals.

For more insight into bone ultrastructure Figures 5 and 6 show AFM images of native and fractured surfaces of trabecular bovine bone. The native surface exhibits bare collagen fibrils (32) with diameters of about 100 nm. These fibrils are composed of a self-assembled bundle of collagen triple-helices, which are 300 nm in length (33). The diameter of the fibrils exhibits a 67 nm periodic modulation along the long fibril axis (33). On the native surface the fibrils exhibit various levels of directional organization, from being strongly parallel to totally disordered. In contrast fracture surfaces exhibit collagen fibrils coated with small platelet-like features, i.e. mineral particles (32, 34, 35) and a much higher overall spatial organization as shown in Figure 6. The collagen fibrils underneath the mineral particles can be uncovered dissolving the particles (32, 35). The crystals can vary in size (10–100 nm) and shape (rounded to lengthy) (35). For a better comparison Figures 5 and 6 are both combined to 3D surface representations given in Figure 7. The fact that fractured surface exhibit mineralized fibrils is presumably due to the fact that during fracture the mineral-mineral interface between neighboring fibrils is the weakest link in the chain (35). These findings and the possibility to perform AFM imaging in a hydrated environment allows functional nano-imaging of bone surfaces. Chemical agents can be used for the stepwise dissection (35) of different bone constituents, giving further insight to the building blocks of bone on the molecular scale. Similar to IGFA, AFM imaging and mechanical testing can be combined for functional biomechanics experiments on the molecular scale. Moreover, with the advent of high-speed AFM imaging (36) such processes can even be monitored in real-time.

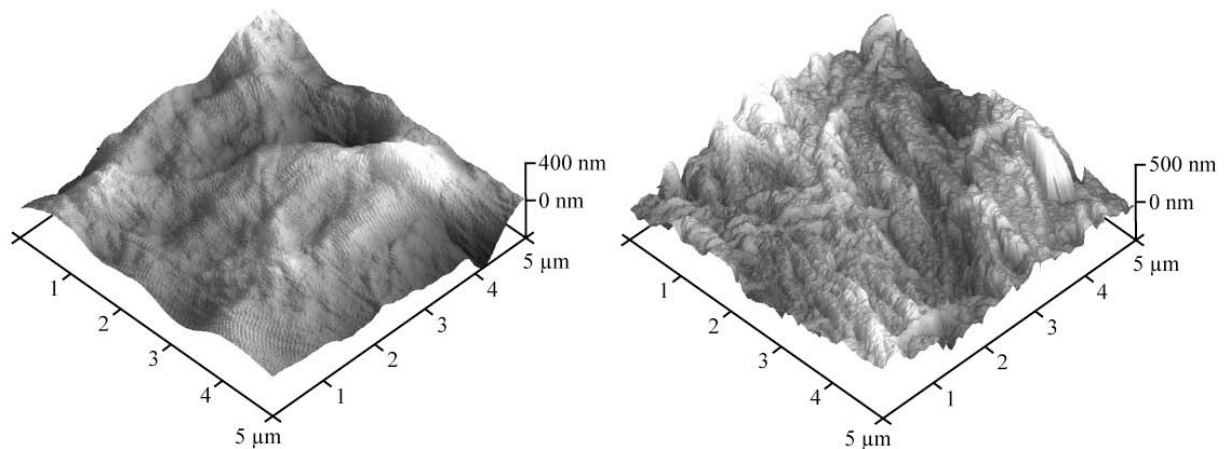


Figure 7: 3D surface plots with mixed height and deflection information of the data shown in Figure 5 and 6.

4. CONCLUSION

In this communication we present novel procedures for improved visualization of trabecular bone. The results obtained from IGFA give indications of the differences between failure of a non-fatigued and a fatigued sample. These indications state that the failure behavior is different and that quantitatively the crack volume encountered is larger in the fatigued case. Moreover, the uncovered details, microcracks and microfractures underline the power of IGFA and SR μ CT as tools to investigate bone failure behavior. The results found shed new light on microcrack investigations and suggest that the classification of cracks in 2D analyses is ambiguous. The majority of detected crack volume is connected to the bone surface and only a very small amount of crack volume is classified as internal cracks. This result is consistent with the strain based failure mode for compact bone found by Nalla et al. (31) and gives rise to the assumption that the microcracks generally initiate at a trabecular bone surface. The results even give an indication of un-cracked ligament bridging. If this result can be validated, SR μ CT might even be used to study toughening mechanisms and the ion-mediated repair process that is associated with them. For investigation of bone on a molecular scale AFM was used, showing the topology of native and fractured bone surfaces. AFM experiments of bone can be done in a functional time lapsed fashion applying either chemical agents or performing in situ mechanical tests. With these tools the new important insights into the nano-composite bone can be gained and potentially lead to a better understanding, diagnosis and therapy of osteoporosis.

ACKNOWLEDGEMENT

We are gratefully indebted to the SNF Grant No. 2153-057127.99, and Postdoctoral fellowship PBEZ2--105116, FWF Project Number J2395-NO2, ÖAW DOC-Fellowship, Veeco/DI Grant Number SB030071, MRL NSF Grant Number DMR00-80034, NASA/URETI Grant Number BiMat NCC-1-02037, USARL (ICB) Grant Number DAAD19-030D-0004, USARIEM (ICB) Grant Number W911QY-04-P-0516 for financial support of this project and to SLS/PSI for beamtime.

REFERENCES

1. Ray, N. F., Chan, J. K., Thamer, M. & Melton, L. J., 3rd Medical expenditures for the treatment of osteoporotic fractures in the United States in 1995: report from the National Osteoporosis Foundation (1997) *J Bone Miner Res* **12**, 24-35.
2. Cooper, C., Atkinson, E. J., Jacobsen, S. J., O'Fallon, W. M. & Melton, L. J., 3rd Population-Based Study of Survival after Osteoporotic Fractures (1993) *Am J Epidemiol* **137**, 1001-5.
3. McElhaney, J. H., Fogle, J. L., Melvin, J. W., Haynes, R. R., Roberts, V. L. & Alem, N. M. Mechanical properties of cranial bone (1970) *J Biomech* **3**, 495-511.
4. Carter, D. R. & Hayes, W. C. The compressive behavior of bone as a two-phase porous structure (1977) *Journal of Bone and Joint Surgery [Am]* **59**, 954-962.
5. Williams, J. L. & Lewis, J. L. Properties and an anisotropic model of cancellous bone from the proximal tibial epiphysis (1982) *J Biomech Eng* **104**, 50-56.
6. Rice, J. C., Cowin, S. C. & Bowman, J. A. On the dependence of the elasticity and strength of cancellous bone on apparent density (1988) *Journal of Biomechanics* **21**, 155-168.
7. Odgaard, A. & Linde, F. The underestimation of Young's modulus in compressive testing of cancellous bone specimens (1991) *Journal of Biomechanics* **24**, 691-698.
8. Keller, T. S. Predicting the compressive mechanical behavior of bone (1994) *J Biomech* **27**, 1159-68.
9. Keaveny, T. M., Guo, X. E., Wachtel, E. F., McMahon, T. A. & Hayes, W. C. Trabecular bone exhibits fully linear elastic behavior and yields at low strains (1994) *Journal of Biomechanics* **27**, 1127-36.
10. Ciarelli, M. J., Goldstein, S. A., Kuhn, J. L., Cody, D. D. & Brown, M. B. Evaluation of orthogonal mechanical properties and density of human trabecular bone from the major metaphyseal regions with materials testing and computed tomography (1991) *J Orthop Res* **9**, 674-82.
11. Marincek, B., Ros, P. R., Reiser, M. & E., B. M. (2000) *Multislice CT - A Practical Guide* (Springer, Berlin, Germany).
12. Weiss, D., Schneider, G., Niemann, B., Guttman, P., Rudolph, D. & Schmahl, G. Computed tomography of cryogenic biological specimens based on X-ray microscopic images (2000) *Ultramicroscopy* **84**, 185-97.
13. Burr, D. B., Martin, R. B., Schaffler, M. B. & Radin, E. L. Bone remodeling in response to in vivo fatigue microdamage (1985) *J Biomech* **18**, 189-200.
14. Burr, D. B., Forwood, M. R., Fyhrle, D. P., Martin, R. B., Schaffler, M. B. & Turner, C. H. Bone microdamage and skeletal fragility in osteoporotic and stress fractures (1997) *J Bone Miner Res* **12**, 6-15.

15. Tantillo, M. & Müller, R. Image-Guided Failure Assessment of Porous Materials (2000) in *Material Research Society Symp. Proc.*, pp. 25 - 30.
16. Muller, R., Gerber, S. C. & Hayes, W. C. Micro-compression: a novel technique for the nondestructive assessment of local bone failure (1998) *Technol Health Care* **6**, 433-44.
17. Nazarian, A. & Muller, R. Time-lapsed microstructural imaging of bone failure behavior (2004) *J Biomech* **37**, 55-65.
18. Hildebrand, T. & Ruegsegger, P. Quantification of bone microarchitecture with the structure model index (1997) *Comput Methods Biomech Biomed Engin* **1**, 15-23.
19. Stampanoni, M., Borchert, G., Wyss, P., Abela, R., Patterson, B., Hunt, S., Vermeulen, D. & Ruegsegger, P. High resolution X-ray detector for synchrotron-based microtomography (2002) *Nuclear Instruments & Methods in Physics Research Section a-Accelerators Spectrometers Detectors and Associated Equipment* **491**, 291-301.
20. Thurner, P., Muller, B. & Beckmann, F. An optimization procedure for spatial and density resolution in hard X-ray micro-computed tomography (2004) *Nuclear Instruments & Methods in Physics Research Section B-Beam Interactions with Materials and Atoms* **225**, 599-603.
21. Weitkamp, T., Rau, C., Snigirev, A. A., Benner, B., Günzler, T. F., Kuhlmann, M. & Schroer, C. G. In-line phase contrast in synchrotron-radiation microradiography and tomography (2002) in *Developments in X-ray Tomography III*, ed. Bonse, U. (SPIE, San Diego), Vol. 4503, pp. 92-102.
22. Thurner, P., Wyss, P., Voide, R., Stauber, M., Muller, B., Stampanoni, M., Hubell, J. A., Muller, R. & Sennhauser, U. (2004) in *Developments in X-Ray tomography IV*, ed. Bonse, U., Denver, Colorado), Vol. 5535, pp. 112-28.
23. Marti, O., Drake, B. & Hansma, P. K. Atomic Force Microscopy of Liquid-Covered Surfaces - Atomic Resolution Images (1987) *Applied Physics Letters* **51**, 484-486.
24. Kindt, J. H., Sitko, J. C., Pietrasanta, L. I., Oroudjev, E., Becker, N., Viani, M. B. & Hansma, H. G. Methods for biological probe microscopy in aqueous fluids (2002) *Atomic Force Microscopy in Cell Biology* **68**, 213-229.
25. Wyss, P., Brönniman, R., Obrist, A., Sennhauser, U., Abela, R. & Stampanoni, M. A sample handler for micrometer resolution X-ray tomographic microscopy (XTM) (submitted) *Review of Scientific Instruments*.
26. Fyhrie, D. P. & Schaffler, M. B. Failure mechanisms in human vertebral cancellous bone (1994) *Bone* **15**, 105-9.
27. Wachtel, E. F. & Keaveny, T. M. Dependence of trabecular damage on mechanical strain (1997) *J Orthop Res* **15**, 781-7.
28. Fazzalari, N. L., Forwood, M. R., Smith, K., Manthey, B. A. & Herreen, P. Assessment of cancellous bone quality in severe osteoarthritis: bone mineral density, mechanics, and microdamage (1998) *Bone* **22**, 381-8.
29. O'Brien, F. J., Taylor, D. & Lee, T. C. Microcrack accumulation at different intervals during fatigue testing of compact bone (2003) *Journal of Biomechanics* **36**, 973-980.
30. Lee, T. C., Arthur, T. L., Gibson, L. J. & Hayes, W. C. Sequential labelling of microdamage in bone using chelating agents (2000) *Journal of Orthopaedic Research* **18**, 322-325.
31. Nalla, R. K., Kinney, J. H. & Ritchie, R. O. Mechanistic fracture criteria for the failure of human cortical bone (2003) *Nat Mater* **2**, 164-8.
32. Hassenkam, T., Fantner, G. E., Cutroni, J. A., Weaver, J. C., Morse, D. E. & Hansma, P. K. High-resolution AFM imaging of intact and fractured trabecular bone (2004) *Bone* **35**, 4-10.
33. Petruska, J. A. & Hodge, A. J. Subunit Model for Tropocollagen Macromolecule (1964) *Proceedings of the National Academy of Sciences of the United States of America* **51**, 871-&.
34. Sasaki, N., Tagami, A., Goto, T., Taniguchi, M., Nakata, M. & Hikichi, K. Atomic force microscopic studies on the structure of bovine femoral cortical bone at the collagen fibril-mineral level (2002) *Journal of Materials Science-Materials in Medicine* **13**, 333-337.
35. Kindt, J. H., Fantner, G. E., Thurner, P. J., Schitter, G. & Hansma, P. K. In-Situ Atomic Force Microscopy of Bone Fracture Surfaces Reveals Collagen Fibrils Individually Coated with Mineral Particles of Varying Shape and Size (2005) *Bone* **submitted**.
36. Schitter, G., Stark, R. W. & Stemmer, A. Fast contact-mode atomic force microscopy on biological specimen by model-based control (2004) *Ultramicroscopy* **100**, 253-257.